Stimulated Raman Emission in Diamond: Spectrum, Gain, and Angular Distribution of Intensity*

A. K. McQuillan,† W. R. L. Clements,‡ and B. P. Stoicheff
Department of Physics, University of Toronto, Toronto, Canada
(Received 10 September 1969)

An experimental study of normal and stimulated Raman emission in diamond is presented, including measurements of linewidth, intensity, and angular distribution of radiation having a frequency shift of 1332.0 cm^{-1}. The diamond crystal formed a Raman resonator; excitation was by a giant-pulse ruby laser. The dependence of normal Stokes emission on laser intensity and the threshold for oscillation were investigated. A value for the Raman gain ($g = 6.9 \times 10^{-3}$ cm^{-1} per MW/cm^2) was calculated from the measured linewidth ($\Delta\nu = 2.04$ cm^{-1}) and cross section for scattering, and found to be in good agreement with a value determined from the threshold for oscillation. The angular distributions of anti-Stokes and Stokes emission and absorption for parallel and convergent laser light are also in good agreement with theory: The emission cone angles are strongly dependent on the angle of convergence of the incident light, and it is established that the preferred directions for emission are those making use of the most intense first-order Stokes radiation which is peaked in the forward direction within the Raman resonator.

INTRODUCTION

Numerous investigations[1] of the anomalous gain, angular distribution of intensity, and spectral linewidths in stimulated Raman emission have been carried out with liquids, and some with gases. Corresponding studies with solids are rare. The first report of stimulated Raman emission in crystals (calcite, diamond, and α sulphur) was given in 1963 by Eckhardt, Bortfeld, and Geller.[2] In 1964, Chiao and Stoicheff[3] made precise measurements of the anti-Stokes emission angles in calcite; Tannenwald[4] (1967) reported the observation of mode pulling in a Raman resonator of crystalline quartz; and Bisson and Mayer[5] (1967–1968) observed an anomalous gain in Raman resonators of calcite, the experimental gain being approximately 10 times the calculated gain.

The present paper deals with the characteristics of the normal and stimulated Raman emission in diamond. Diamond is particularly well suited for stimulated Raman experiments since the first-order Raman spectrum is known[6] to consist of a single sharp line of relatively high intensity. Therefore, the threshold for stimulated emission is expected to be low. The available diamond crystal was in the form of a plate with parallel surfaces and, because of the large refractive index of diamond, the plate served as a resonator. Thus, our experimental results have been strongly influenced by the properties of this resonator.

The main results of our investigations have been reported briefly on various occasions.[7] The linewidth and scattering cross section were determined from the normal Raman spectrum. The intensity of normal Stokes emission was found to increase linearly with increasing laser intensity up to threshold for stimulated emission; this region was followed by a sharp increase in intensity by a factor of $\sim 10^6$, and eventually by saturation and damage to the crystal. In a resonator, the onset of oscillation is governed by the condition $Fe^{(g-\alpha)L} = 1$, where F is the feedback factor, g and α are the gain and loss constants, and L is the crystal length. This condition was used to determine a value for the gain from the observed threshold for oscillation. A thorough study of the inhomogeneous intensity distribution of laser and Stokes radiation in the resonator was also carried out in order to properly evaluate the gain constant. Good agreement was found between the value determined in this way, and that value calculated from the measured scattering cross section and linewidth. Self-focusing was not apparent nor was stimulated Brillouin scattering detected at the power levels used in these experiments. The stimulated linewidth was observed to be an order of magnitude narrower than the normal linewidth, and on occasion two axial components of the Raman resonator were observed, with evidence of mode pulling and strong mode interaction.

The angular distribution of intensity in the stimulated Raman emission was discussed in some of the first papers on the theory of the process.[8–10] From the momentum-matching condition based on a plane-wave model, maxima of anti-Stokes and Stokes emission (and the corresponding minima in first-order Stokes emission) are predicted according to the wave-vector relations

$$\vec{k}_0+\vec{k}_{n-1}=\vec{k}_{-1}+\vec{k}_n;\quad \vec{k}_0+\vec{k}_{-1}=\vec{k}_{n-1}+\vec{k}_{-n}. \tag{1}$$

Here $\vec{k}_0$, $\vec{k}_{-1}$, $\vec{k}_n$, and $\vec{k}_{-n}$ are, respectively, the laser, the first Stokes, the nth-order anti-Stokes, and the Stokes wave vectors. Such distribution of intensity in calcite was investigated by Chiao and Stoicheff,[3] who found that agreement between the observed and calculated cone angles was within the experimental error of a few percent, when an essentially parallel laser beam was incident on the calcite. In addition, they noted a significant increase in emission angles of anti-Stokes radiation as the focal length of the lens used to focus the laser beam was decreased. Shimoda[11] has discussed such an increase in cone angle with increase in angle of convergence of the laser beam; and Bloembergen and Shen[12] have considered multimode effects, where two laser modes, with a relative angle θ, result in broadened anti-Stokes emission cones with an increase in apex half-angle of about $\frac{1}{2}\theta$. We have made a detailed study of the angular dependence of anti-Stokes and Stokes radiation in diamond and investigated in particular the changes in cone angles with different beam apertures and different beam convergence.

EXPERIMENTAL PROCEDURE

The crystal of type-II A diamond was in the form of a plate 2.18 mm thick and with flat, highly polished, and almost parallel surfaces (wedge angle ~10′). Diamond has a refractive index of 2.4; thus, the reflectivity at the air surfaces is 17% and the plate behaves as a Raman resonator. A Laue x-ray diffraction photograph established that the [111] axis of the crystal was approximately perpendicular to the polished faces of the diamond plate.

For measurement of the normal Raman linewidth, the spectrum was excited by λ 6328 radiation of a He-Ne laser and analyzed with a Fabry-Perot interferometer, as described by Clements and Stoicheff.[13] In this experiment, the Fabry-Perot spacer was 0.869 ± 0.003 mm, mirror reflectivity was 99%, and total laser plus instrumental width was 0.064 cm^{-1}. The scattered light was observed at right angles to the incident beam.

Stimulated Raman emission was excited by λ 6940 radiation from a giant-pulse ruby laser. The radiation was plane polarized and was emitted in a single pulse of ~30-nsec duration and in a single (or nearly single) axial mode. Good reproducibility in the laser pulse was obtained by firing the laser at constant power near threshold at regular intervals with the ruby at a constant temperature (−10 °C).

The experimental arrangement for photographing the stimulated Raman spectrum and for measuring its intensity is shown in Fig. 1. Laser radiation was incident on an aperture of 3.6 mm diam and

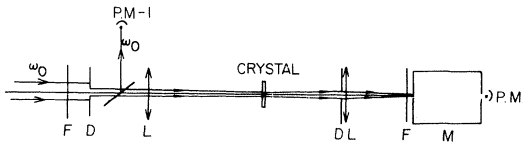

FIG. 1. Schematic diagram of apparatus for intensity measurements. Explanation of symbols: F, attenuating filter; D, diaphragm; L, lens; M, spectrometer; PM, photomultiplier detector.

its intensity was measured by a 931A (RCA) phototube. A lens of 18-cm focal length was used to focus the laser beam 2 cm beyond the diamond crystal. Radiation scattered in the forward direction was focused on the slit of the grating spectrograph. Photographs of the Raman spectrum were obtained with a 1-cm^{-1} slit width and a 20-cm^{-1}/mm reciprocal linear dispersion. Some photographs were also obtained at much higher resolution, with the spectrograph replaced by a Fabry-Perot interferometer and a 1-m camera lens.

For measuring the intensity of first-order Stokes radiation, the method used was that described in a recent study in this laboratory[14] of intensity measurements in liquid O_2 and N_2. The laser radiation was varied by inserting neutral density filters in the beam at the entrance aperture. Radiation scattered in a cone of 3.9×10^{-3} sr was collected through an aperture and focused on the slit of the spectrometer. A 7102 (RCA) phototube was used to detect the Stokes radiation, and the Stokes and laser signals were displayed on a dual oscilloscope (Tektronix 555). The pulse heights gave effective measurements of the Stokes and laser intensities. The transmission characteristics of the spectrometer and attenuating filters, as well as the sensitivity of the phototubes, were determined, and the complete arrangement was calibrated by measurements with benzene, all as described in the earlier work.[14] The measured Raman intensity is estimated to be accurate to ±30%.

For observation of the angular distribution of intensity, the same arrangement as in Fig. 1 was used but with the optical elements after the diamond crystal replaced by a camera. Appropriate filters were placed in front of the camera to isolate the various Stokes and anti-Stokes frequency components.

SPECTRUM

The normal Raman spectrum of the diamond crystal consists of a single line at a frequency shift of 1332 cm^{-1}. This line was found to have a Lorentzian line shape with full width at half-intensity-maximum measured to be 2.04 ± 0.04 cm^{-1} at room temperature. Measurements of the linewidths exhibited by two other diamond crystals (al-

FIG. 2. Fabry-Perot interferogram of Stokes radiation showing two oscillating modes separated by ~ 0.3 cm^{-1}. The interorder spacing is ~ 3 cm^{-1}.

so type-II) gave similar values, namely 2.09 ± 0.04 and 2.22 ± 0.04 cm^{-1}.

Photographs of the stimulated Raman spectrum of diamond revealed four sharp lines, two being the first- and second-order Stokes lines and two the corresponding anti-Stokes lines. Their frequency shifts from the exciting line were measured to be 1331.8 ± 2 cm^{-1} and double this value, corresponding to the fundamental and exact multiple of the C-C vibrational frequency. Examination of the first-order Stokes line at high resolution with a Fabry-Perot interferometer (Fig. 2) showed that its width was very narrow, with variation of 0.1 to 0.2 cm^{-1}, from shot to shot of the laser. This spectral width is at least $\frac{1}{10}$ that of the normal Raman line, yet it is considerably larger than that of the laser exciting line.

In approximately 10% of these photographs the stimulated Stokes line was split into two components separated by 0.35 ± 0.15 cm^{-1} (Fig. 2) while the laser exciting line itself remained single and sharp. Further study of the spectrum, with the emission region of the crystal magnified 20X (Fig. 3) and 100X revealed the presence of many regions of oscillation, each approximately 50 μ wide and 100–150 μ long. Their size was governed partly by the multiple-beam interference fringes with spacing $\lambda/(2n\delta) \approx 55$ μ, corresponding to the 10′-tilt δ between the polished faces of the crystal, and perhaps also due to imperfect surfaces or to the existence of many crystallites. (Spectra observed with a tilted Fabry-Perot interferometer and 100X magnification indicated that these regions sometimes oscillated independently of one another, some in a single mode, others in two axial modes, with the magnitude of the splitting and the intensity ratio of the two modes varying from region to region.)

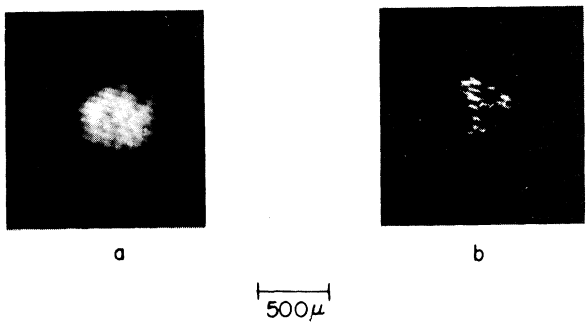

FIG. 3. Near-field patterns of (a) laser radiation in the diamond crystal below threshold for stimulated Raman emission and (b) stimulated Stokes radiation.

The average mode separation in our diamond resonator is $1/(2nL) \approx 1$ cm^{-1}, which is approximately half the normal Raman linewidth. Under these conditions there should be strong mode pulling, as observed by Tannenwald[4] in Raman resonators of quartz. Mode pulling would be expected to decrease the mode separation by the factor $(1 - \Delta\nu_C/\Delta\nu_a)$, where $\Delta\nu_a$ is the normal Raman linewidth and $\Delta\nu_C$ is the cavity linewidth defined in the usual way as $\Delta\nu_C = \alpha'/(2\pi nL)$, with α' the fractional power loss $(1 - R)$ at the cavity surfaces. For ideal surfaces $\Delta\nu_C \sim 0.3$ cm^{-1}, however, as shown by the width of the fringes in Fig. 3, the value for our crystal is approximately twice this value, that is, $\Delta\nu_C \approx 0.6$ cm^{-1}. This would lead to a decrease of the mode separation from a value of ~ 1 cm^{-1} to ~ 0.7 cm^{-1}, still somewhat larger than the observed separations in the range 0.2–0.5 cm^{-1}. Further decrease could arise from an absorption loss[4] related to focusing geometry or from strong electric-field interaction effects as observed in gas lasers[15] when the cavity mode spacing and the normal (spontaneous) linewidth are almost the same, as in the present experiment.

INTENSITY OF STOKES RADIATION AND RAMAN GAIN

The observed intensity of first-order Stokes radiation and its dependence on incident laser intensity is shown in the graph of Fig. 4. At low laser power, normal Raman emission was observed, this increased linearly with increasing laser power. The threshold for oscillation occurred at a laser power of 1.05 MW, and Stokes intensity increased sharply by a factor of about 10^6 for an increase in laser power to 1.5 MW. At higher laser powers, saturation set in and further increase resulted in damage to the crystal.

The region of normal Raman emission is shown in more detail in Fig. 5, which clearly illustrates the linear increase of Stokes power with increasing laser power. The measured slope of this graph was used to obtain a value for the total Raman scattering efficiency S, which is defined as the ratio of the number of scattered photons at frequency ω_S (produced per unit time per unit cross-sectional area of crystal in a solid angle Ω about the di-

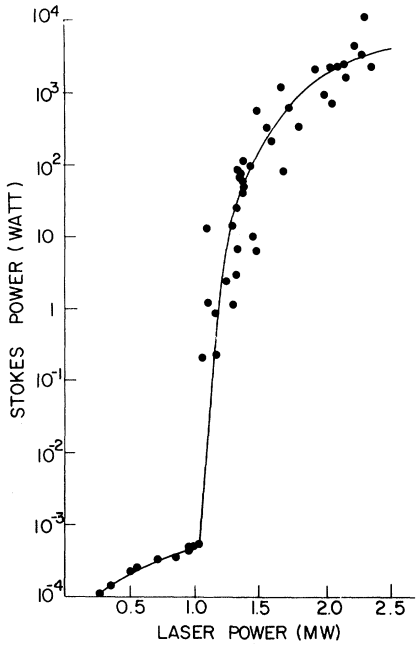

FIG. 4. Experimental curve of Raman-Stokes power versus incident laser power.

rection of observation) to the number of incident photons of frequency ω_0 crossing unit area in unit time. The experimental value of S is given by $(P_\gamma/P_0)(1/L\Omega)$, where P_γ is the Raman power for the whole Raman line scattered into the solid angle Ω, P_0 is the corresponding laser power, and L is the path length. A value of $S = 2.7\times10^{-7}$ cm^{-1} sr^{-1} was obtained, having an estimated accuracy of $\pm 30\%$. Now S is related to $d\alpha/dx$, the rate of change of electronic polarizability per unit cell with relative displacement of the atoms, according to Smith[16] and Loudon,[17] is given by

$$S = \frac{3hN^2\omega_s^4}{2\pi c^4\rho\omega_0}\left|\frac{d\alpha}{dx}\right|^2(n_0+1) \ .$$

Here $\omega_S = \omega 0 - \omega_\gamma$ is the Stokes angular frequency, ω_0 is the laser frequency, and $\omega_\gamma = 1332$ cm^{-1}; N is the number of unit cells per unit volume, n_0 is the Bose population factor (with $n_0+1 \sim 1$ at room temperature), and ρ is the crystal density. From the above value of S, we obtain $d\alpha/dx = 4.6\times10^{-16}$ cm^2 per unit cell, for laser radiation propagating along the [111] axis of the crystal. This value is in good agreement with the value 4.0×10^{-16} cm^2 obtained by Anastassakis, Iwasa, and Burstein[18] from electric-field-induced infrared absorption in diamond.

The Raman gain per unit length of active medium is defined by

$$g = 16\pi^2c^2S_{\|}I_0/hn^2\omega_s{}^3\Delta\nu \ .$$

Here, $S_\|$ is the scattering efficiency of radiation polarized in the same plane as the incident plane-polarized laser radiation and equals $S/(1+d)$, where d $(=I_\perp/I_\|)$ is the depolarization ratio; $\Delta\nu$ (cm^{-1}) is the full width at half-intensity of the normal Raman line, n is the refractive index of the medium, I_0 is the incident laser intensity, and the remaining symbols have their usual meanings. With the above experimental values of $S = 2.7\times10^{-7}$ cm^{-1} sr^{-1}, $d = 0.60$, and $\Delta\nu = 2.04$ cm^{-1}, the Raman gain in diamond is calculated to be $g = 6.9\times10^{-3}I_0$ cm^{-1} with I_0 in MW/cm^2.

This value for the Raman gain determined entirely from the characteristics of the normal Raman spectrum can now be tested with the observed threshold for oscillation. As already noted in the Introduction, the condition for oscillation threshold is $F\exp[(g-\alpha)L] = 1$. The feedback factor $F \equiv$ reflectivity $= 0.17$; the loss constant α was considered to be negligible (since the observed scattering and absorption losses at low intensities with the ruby laser were small), and diffraction losses for such a small path length are also expected to be small relative to g. Thus, the threshold condition reduces to $e^{gL} = 5.9 = e^{1.8}$, or $gL = 1.8$; that is, at threshold, $g = 8.2$ cm^{-1}. From the above values, $g = 8.2 = 6.9\times10^{-3}\,I_0$, the laser intensity at threshold would be expected to be $I_0 \approx 1200$ MW/cm^2.

According to Fig. 4 the laser power at threshold as measured by PM-1 is 1.05 MW. The spatial intensity distribution of the laser and Stokes radiation was investigated by taking near-field photographs (at magnification of 20X) of the illuminated area of the crystal. The laser beam cross-sectional area at the crystal was measured to be 0.37 mm^2: However, the area of maximum intensity was determined to be 0.2 mm^2 (by interposing neutral density filters in the beam) and this area is shown in Fig. 3.

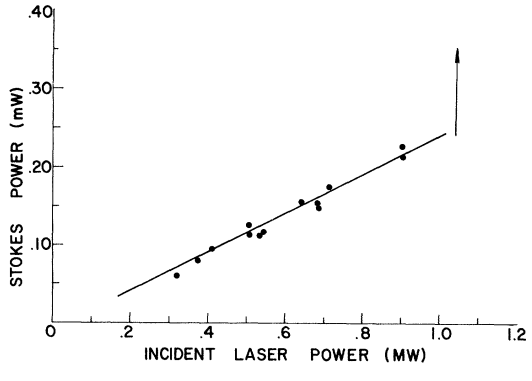

FIG. 5. Experimental curve of normal Raman scattering power versus incident laser power. The arrow indicates the onset of oscillation.

Accordingly the laser intensity incident on the crystal at threshold is $1.05/0.002 \approx 530$ MW/cm^2. The intensity within the crystal, however, is modified because the crystal forms a resonator. This behavior is evident in the near-field photographs (Fig. 3) of both the laser and Stokes radiation, which show interference fringes with spacing $\approx 55\ \mu$, caused by the slight wedge between the polished faces of the crystal. For such multiple-beam interference, the fringe maxima have intensity equal to that of the incident light I_0 and the minima have intensity $[(1-R)/(1+R)]^2 \approx 0.5I_0$ for diamond with 17% reflectivity. Also, the finesse ≈ 1.5, that is, the fringe width is somewhat less than the fringe spacing (Fig. 3). At threshold, only the intensity maxima, comprising at most half the laser-beam area at the crystal, will be effective in generating stimulated Stokes radiation. Therefore, according to this analysis, the laser intensity at threshold is at least 530/0.5 or ~ 1100 MW/cm^2. This apparently excellent agreement with the expected value of ~1200 MW/cm^2 is, no doubt, fortuitous; the experimental values of S and $S_{||}$ have accuracies of ~30%, and intensity peaks in the fringe maxima of the laser radiation are indicative of spatial inhomogeneity in the laser beam. In spite of these uncertainties, the observed low oscillation threshold in diamond appears to be within a factor of about 2 of the value calculated from the Raman gain $g = 6.9 \times 10^{-3}\ I_0$.

ANGULAR DISTRIBUTION OF INTENSITY

Owing to the thinness of the diamond crystal available, some focusing of the incident laser light was necessary to observe stimulated emission. With the use of a long focal-length lens ($f \approx 30$ cm) and almost parallel exciting radiation, the emission cones of the first three orders of anti-Stokes and of the second-order Stokes radiation were observed along with the corresponding intensity minima in the diffuse first-order Stokes emission. The measured values of the cone angles are given in Table I and, for comparison, the values calculated from Eq. (1) are included. In these calculations tabulated values of the refractive index over the wavelength range 4861 Å to 7593 Å were used.[19] It is seen that the agreement is very good for all of the emission angles observed, although not as good for the Stokes minima, which were difficult to measure. We conclude that, just as for calcite, the theory of the plane-wave phase matching conditions is applicable to diamond.

No intensity-dependent change in cone angles was observed at incident laser-power densities from threshold up to 2.5 times threshold. Although an intensity dependence in the direction of maximum anti-Stokes intensity has been predicted by Bloembergen and Shen,[9] the theoretical change in cone half-angle over this range is ~ 2×10^{-3} rad. The necessity of using strongly convergent incident light (convergence angle 0.023 rad) to cover this intensity range, and the broadness of the anti-Stokes rings, makes comparison with theory inconclusive.

The cone angles are very sensitively dependent on the angle of convergence of the incident laser beam even at threshold. A series of experiments was carried out in which the laser radiation was focused by lenses of different focal lengths and then incident on the diamond crystal. Focal lengths of 2.7, 3.3, 5.2, 9.8, 17.4, 26.0, 31.0, and 50.0 cm were used and, as before, photographs of the first- and second-order anti-Stokes and of the second-order Stokes "rings" were obtained. The corresponding angles are plotted against the reciprocal of the focal length in Fig. 6. A linear relation is evident for the anti-Stokes cone angles, with the angles increasing as the focal length becomes shorter: thus, $\theta_{AS} \propto 1/f$. However, the second-order Stokes cone angles show a completely different dependence on focal length. The angle decreases sharply with shorter focal lengths and appears to reach a limiting value of about 0.065 rad.

In another series of experiments the dependence of the cone angles on the aperture of the incident radiation was investigated. A lens with $f = 5.15$ cm was used to focus the laser beam. Apertures of 1.0, 1.6, 1.9, 2.4, 2.8, and 3.6 mm diam were placed in turn at the center of the lens, and photographs of the rings were obtained. The results are shown in a graph of anti-Stokes cone angle versus aperture diam in Fig. 7. The results clearly indicate a linear relation $\theta_{AS} \propto d$.

TABLE I. Comparison of theoretical and experimental values of the emission and absorption angles (in radians) observed in diamond.

Frequency	Emission angles		Absorption angles	
	Expt	Theory	Expt	Theory
$\omega_0 - 2\omega_\gamma$	0.116	0.119	(0.048)[a]	0.043
$\omega_0 + \omega_\gamma$	0.053	0.053	0.060	0.064
$\omega_0 + 2\omega_\gamma$	0.103	0.104	(0.079)	0.071
$\omega_0 + 3\omega_\gamma$	0.158	0.152	•••	0.079

[a]Values in brackets are measurements of weak and broad absorption rings.

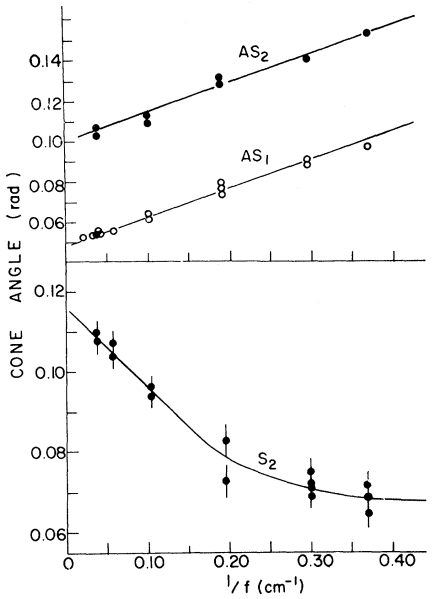

FIG. 6. Graphs of emission angles observed for first- and second-order anti-Stokes (AS_1 and AS_2) and for second-order Stokes (S_2) radiation as a function of inverse focal lengths of lenses used to focus laser radiation.

These two series of experiments establish the result that the cone angles of anti-Stokes emission depend on the angle of convergence of the incident exciting radiation. More precisely, the change in angle is given by $\Delta\theta_{AS} = K(a/f)$, where K is a constant, a the aperture radius, and f the focal length. The first anti-Stokes cone angles are therefore given by $\theta_{AS} = 0.053 + K(a/f)$, where a/f defines the cone angle of the periphery of the converging laser beam. This result implies that the wave vector relations of Eq. (1) are rotated by the angle $K(a/f)$, as shown in Fig. 8. The numerical value of K is 0.9 ± 0.2.

According to the theory of the stimulated Raman process, anti-Stokes radiation is generated by terms of the form $\chi_a E_0^2 E_S$, where χ_a is the susceptibility at $\omega_0 + \omega_\gamma$ and E_0 and E_S are the electric fields at ω_0 and $\omega_0 - \omega_\gamma$. The generation of anti-Stokes radiation is coupled to Stokes radiation and the direction of maximum intensity will depend on the direction of maximum intensity of laser and Stokes radiation. Once these directions have been established, the anti-Stokes cone angles can be determined from the momentum-matching condition.

All of our observations can be explained in this way provided that first-order Stokes radiation is predominantly in the forward direction. This condition was satisfied in our experiment; the diamond was set with polished faces approximately perpendicular to the beam axis so that when either parallel or convergent light was incident on the crystal, Stokes radiation along the beam axis was favored. Also, spurious scattering of Stokes radiation within the crystal or at its surfaces ensured the presence of Stokes radiation at half-angles of $\sim 6°$ to the forward direction.

When laser and Stokes radiation interact to produce anti-Stokes emission, that direction will be preferred which makes use of intense Stokes radiation closest to the resonator axis. With a converging incident beam it is possible to couple Stokes closer to the axis and still satisfy the phase matching conditions. This results in an increase in anti-Stokes emission angle with a/f, up to the extreme case of anti-Stokes emission at $0.053 + 0.064$ rad (see Table I) and Stokes radiation on axis. Experiments were performed to observe the

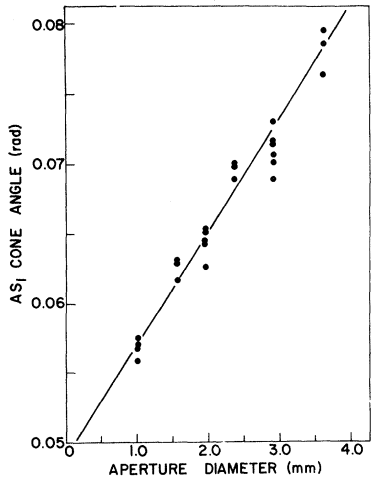

FIG. 7. Graph of first-order anti-Stokes emission angle as a function of limiting aperture diameter of converging laser beam.

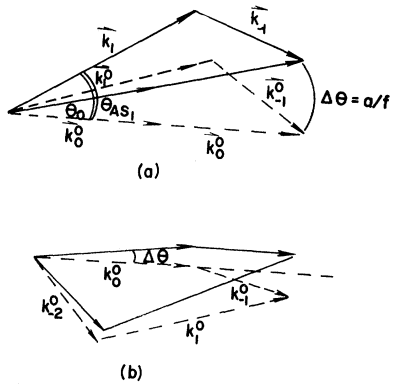

FIG. 8. Diagrams of changes in (a) first-order anti-Stokes emission angle, and (b) second-order Stokes emission angle, with change in direction of first-order Stokes wave vector $\vec{k}_{-1}$.

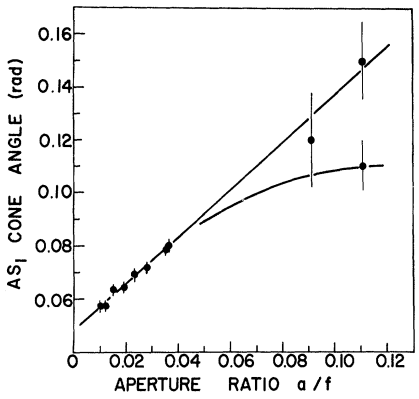

FIG. 9. Graph of first-order anti-Stokes emission angle as a function of convergence angle of incident laser beam.

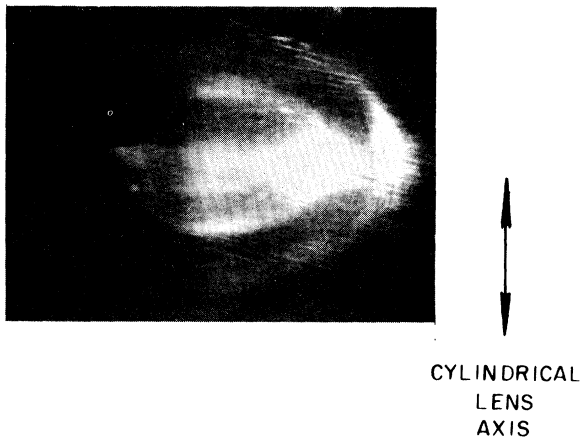

FIG. 10. Elliptical anti-Stokes radiation pattern obtained by focusing laser beam with a cylindrical lens.

behavior of the anti-Stokes emission at values of a/f greater than 0.064 (Fig. 9). Convergence angles of 0.091 and 0.112 were used. In both cases the system was somewhat "confused," giving very broad emissions. With a convergence angle of 0.112 rad, two maxima were present in the anti-Stokes emission. The more intense one corresponded to a cone angle of about 0.11 rad (with Stokes along the axis), and the weaker ring corresponded to an angle of 0.15 rad (with Stokes slightly off-axis and laser radiation at the periphery of the beam).

The dependence of the second-order Stokes emission angle on convergence of the laser beam further illustrates the preference of the higher-order Raman emissions to couple to Stokes close to the axis. From the wave-vector diagram in Fig. 8, it is seen that, with increasing angle of the laser radiation, first-order Stokes radiation closer to the axis is effective in producing second-order Stokes emission. However, the emission angle decreases with increasing angle of convergence of laser radiation. It appears to reach a limiting value of about 0.07 rad ($\sim 0.116 - 0.043$) with Stokes radiation on axis. This explains the observed behavior shown in Fig. 6.

It is also evident from the above explanation of the importance of beam convergence, that when a cylindrical lens (or a spherical lens with a long slit as aperture) is used to focus the laser beam, the "ring" pattern will be replaced by "elliptical" patterns, the minor axis being determined by the cylinder axis (or width of slit). Moreover, maxima of intensity will occur at the extremities of the major axis produced by converging light, since the gain would be largest for Stokes radiation closest to the beam axis. Elliptical patterns exhibiting these features have been observed with calcite and with class-I radiation in liquids.[20] An example of such a pattern obtained by focusing with a cylindrical lens in diamond is shown in Fig. 10.

CONCLUSIONS

The present investigation has combined the study of the stimulated Raman effect in a solid with the behavior of a Raman oscillator. As in an earlier study with liquid O_2 and N_2, the stimulated Raman effect in diamond is simplified by the absence of self-focusing and stimulated Brillouin scattering. The experimental results are consistent with theory. This study of the angular properties of stimulated emission confirms the earlier results obtained with calcite and extends our knowledge of the production of class-I radiation in solids. Also, in this study, the value of the Raman gain determined from the measured cross section and linewidth of normal Raman scattering gives an oscillation threshold which is in reasonable agreement with the observed value.

ACKNOWLEDGMENTS

We are grateful to Dr. J. B. Grun for assistance with the intensity measurements and to Dr. R. H. Stolen and Dr. F. Shimizu for valuable discussions.

*This research is part of Project DEFENDER under the joint sponsorship of the Advanced Research Projects Agency, the U. S. Office of Naval Research and the Department of Defense. It is also supported by the National Research Council of Canada and the University of Toronto.

†Holder of Province of Ontario Government Scholarships 1965–68; Present address: Department of Physics, York University, Toronto, Canada.

‡Holder of Province of Ontario Government Scholar-

ships 1968–69.
[1]N. Bloembergen, Am. J. Phys. 35, 989 (1967).
[2]G. Eckhardt, D. P. Bortfeld, and M. Geller, Appl. Phys. Letters 3, 137 (1963).
[3]R. Y. Chiao and B. P. Stoicheff, Phys. Rev. Letters 12, 290 (1964).
[4]P. E. Tannenwald, J. Appl. Phys. 38, 4788 (1967).
[5]G. Bisson and G. Mayer, C. R. Acad. Sci. Paris 265, 397 (1967); J. Phys. 29, 97 (1968).
[6]R. S. Krishnan, Proc. Indian Acad. Sci. A24, 45 (1946).
[7]A. K. McQuillan and B. P. Stoicheff, Bull. Am. Phys. Soc. 12, 60 (1967); IEEE J. Quant. Electron. QE-4, 381 (1968).
[8]E. Garmire, E. Panderese, and C. H. Townes, Phys. Rev. Letters 11, 160 (1963).
[9]N. Bloembergen and Y. R. Shen, Phys. Rev. Letters 12, 504 (1964); Phys. Rev. 137, A1787 (1965).
[10]P. D. Maker and R. W. Terhune, Phys. Rev. 137, A801 (1965).
[11]K. Shimoda, J. Appl. Phys. Japan 5, 86 (1966).
[12]N. Bloembergen and Y. R. Shen, Phys. Rev. Letters 13, 720 (1964).
[13]W. R. L. Clements and B. P. Stoicheff, Appl. Phys. Letters 12, 246 (1968).
[14]J. B. Grun, A. K. McQuillan, and B. P. Stoicheff, Phys. Rev. 180, 61 (1969).
[15]W. J. Witteman, Phys. Rev. 143, 316 (1966).
[16]H. M. J. Smith, Phil. Trans. Roy. Soc. A241, 105 (1948).
[17]R. Loudon, Advan. Phys. 13, 423 (1964).
[18]E. Anastassakis, S. Iwasa, and E. Burstein, Phys. Rev. Letters 17, 1051 (1966).
[19] Landolt-Bornstein, Physik.-Chem. Tabellen (Julius Springer-Verlag, Berlin, 1923), Vol. II, p. 918.
[20]E. Garmire, Phys. Letters 17, 251 (1965); in Physics of Quantum Electronics, edited by P. L. Kelley, B. Lax, and P. E. Tannenwald (McGraw-Hill Book Co., New York, 1966), pp. 167–179.

PHYSICAL REVIEW A VOLUME 1, NUMBER 4 MARCH 1970

Generalizations of Gaussian Optical Fields

B. Picinbono and M. Rousseau
Institut d'Electronique Fondamentale, Faculté des Sciences, 91-Orsay, France*
(Received 26 June 1969)

Stationary Gaussian optical fields are also often called thermal fields because they are generated by natural or thermal sources. By using the amplitude of the field, we show that thermal fields are only a particular case of the more general class of Gaussian fields. Such nonthermal Gaussian fields can be obtained experimentally, and we calculate some properties, concerning particularly the effect of Hanbury Brown and Twiss, photocounting, and coincidence experiments. We show that the thermal fields are the less chaotic or incoherent Gaussian fields. Finally, we introduce pseudo-Gaussian fields which appear in some experiments of diffusion with laser light. They are non-Gaussian fields, but their intensity has the same properties as that of a Gaussian field.

I. INTRODUCTION

Statistical properties of optical fields have been extensively studied in recent years. In particular, we now have very good descriptions of coherence, photon coincidence, and photocounting experiments.[1–3] These descriptions can be achieved by using classical concepts, where the statistical nature of the electromagnetic field is described by means of an appropriate stochastic process. Coherence properties are thus defined by a set of coherence functions which are particular moments of the process. However, the statistical nature of the field is also described quantum-mechanically by a density matrix which allows us to introduce quantum coherence functions.

The correspondence, which is in some cases an equivalence between the classical and the quantum description, can be studied by using coherent states and the P representation. The main result of this study is that, even though the quantum description is more appropriate to a microscopic description, the two points of view are completely equivalent in the case of fields actually studied in the laboratory.[4] Theoretically, there are fields which have no classical equivalence,[5] but up to now they have not been obtained experimentally.

This is particularly the case for natural light and laser light. Ideal laser (or coherent) light is represented by a coherent state or by a nonrandom function of time. Thermal (or Gaussian or chaotic) light is generated by a natural source, and its Gaussian properties appear as a consequence of the central-limit theorem.[6] This statement is also

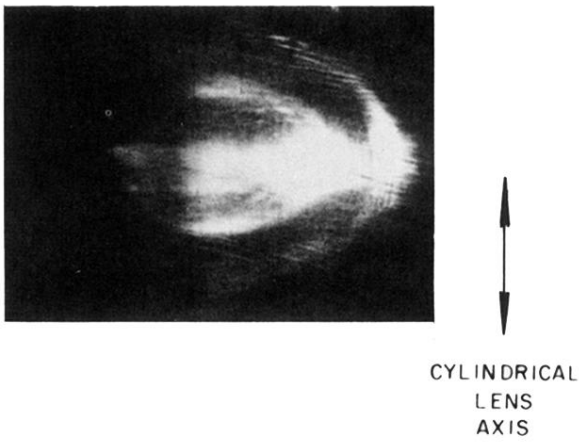

FIG. 10. Elliptical anti-Stokes radiation pattern obtained by focusing laser beam with a cylindrical lens.

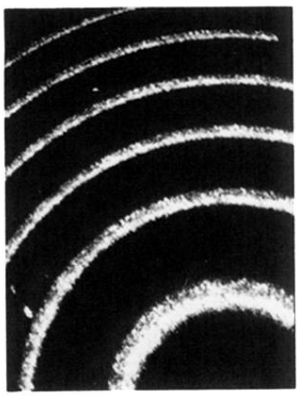

FIG. 2. Fabry-Perot interferogram of Stokes radiation showing two oscillating modes separated by ~ 0.3 cm^{-1}. The interorder spacing is ~ 3 cm^{-1}.

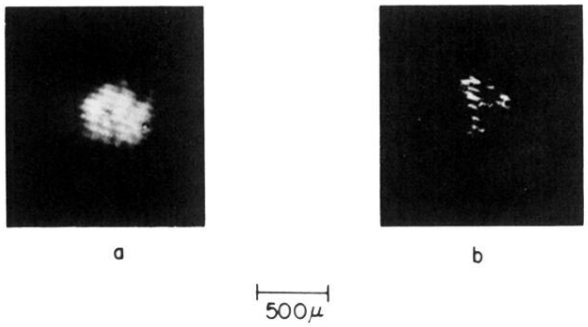

FIG. 3. Near-field patterns of (a) laser radiation in the diamond crystal below threshold for stimulated Raman emission and (b) stimulated Stokes radiation.